


Probing giant Zeeman shift in vanadium-doped WSe₂ via resonant magnetotunneling transportJinbao Jiang,^{1,2,*} Lan-Anh T. Nguyen,^{1,2,*} Tuan Dung Nguyen,^{1,2} Dinh Hoa Luong,^{1,2} Duk Young Kim,¹ Youngjo Jin,^{1,3} Philip Kim,³ Dinh Loc Duong,^{1,2,†} and Young Hee Lee^{1,2,4,‡}¹Center for Integrated Nanostructure Physics (CINAP), Institute for Basic Science (IBS), Suwon 16419, Republic of Korea²Department of Energy Science, Sungkyunkwan University, Suwon 16419, Republic of Korea³Department of Physics, Harvard University, Cambridge, Massachusetts 02138, USA⁴Department of Physics, Sungkyunkwan University, Suwon 16419, Republic of Korea (Received 3 November 2020; revised 7 January 2021; accepted 11 January 2021; published 26 January 2021)

Doping van der Waals layered semiconductors with magnetic atoms is a simple and effective approach to induce magnetism. However, investigation of the electrical properties of such two-dimensional semiconductors and the modulation of their magnetic order for spintronics is still lacking. Herein, we report a giant Zeeman shift from the spin-polarized state in tungsten diselenide (WSe₂) doped with a small amount of vanadium (V) atoms (~0.1%). The Zeeman shift was measured via resonant magnetotunneling spectroscopy with a vertical graphite/V-WSe₂/graphite heterojunction. The *p*-type doping state near the valence band is substantially shifted under an external magnetic field by 7.8 meV/T, equivalent to a giant *g* factor of approximately 135, an order of magnitude higher than that of other two-dimensional magnetic semiconductors. The ferromagnetic order of the spin glass state and its long-range interaction are revealed by the remanence of magnetoresistance between the zero-field cooling and field-cooling processes as well as magnetoresistance hysteresis. The ferromagnetic glass order is fully established at 50 K, whereas the long-range interaction persists at higher temperatures of up to 300 K in V-doped WSe₂ flakes with an approximate thickness of 5 nm. Our work sheds light on the magnetic nature of V-doped WSe₂ semiconductors and paves the way for future spintronics based on two-dimensional van der Waals magnetic semiconductors.

DOI: [10.1103/PhysRevB.103.014441](https://doi.org/10.1103/PhysRevB.103.014441)**I. INTRODUCTION**

The incorporation of magnetic dopants into semiconductors is a versatile approach to provoke spin-charge interaction, and the magnetic order in such doped semiconductors can be controlled by an external current or a gate bias [1–9]. The magnetic dopant not only creates localized doping states but also generates spin-polarized states by strongly hybridizing with the host states [3,10,11], forming spin clusters with a size below 1 nm via short-range exchange interactions [12,13]. If such local spin clusters interact with each other via free carriers (e.g., RKKY interaction) [13–16], for example, a long-range magnetic order can be established by tuning free-carrier concentration [17]. The magnetic order can also be realized via short-range interactions if the doping concentration is sufficiently high to ensure that dopants are in close proximity; however, in this case, the magnetic order cannot be modulated by adjusting the gate bias [18]. Therefore, the doping concentration is often expected to be low (approximately 10¹² cm⁻² or 10¹⁸ cm⁻³) to enable the magnetic order in semiconductors to be modulated. The term “diluted magnetic semiconductors” (DMSs) is used to describe these materials. The issue is how to choose a proper magnetic dopant for a cer-

tain semiconductor host, which can satisfy above-mentioned conditions (formation of long-range magnetic order with low doping concentration). A typical material in this regard is Mn-doped GaAs [19,20] with a Curie temperature (*T_c*) of 190 K and a substantially high doping concentration of ~10% Mn [21–24]. The magnetic order in this material is formed via direct interaction between dopant atoms; this is known as the impurity model [25–27].

Two-dimensional (2D) van der Waals (vdW) layered semiconductors have recently been investigated to obtain 2D DMSs. A variety of 2D vdW semiconductors have given rise to opportunities to obtain realistic DMSs [28–38]. Although Fe or Mn atoms have been introduced as dopants in 2D vdW host semiconductors, both of these dopants create midgap states, pinning the Fermi level inside the bandgap [29,30,39–41]. Such band structures cannot generate a long-range magnetic order at high temperatures, as observed in experiments [41]. Recently, circularly polarized photoluminescence (PL) was used in Fe-doped MoS₂ to confirm the existence of ferromagnetism; however, this is questionable because of the purported PL emission above the bandgap of MoS₂ [36]. In contrast, vanadium-doped WSe₂ (V-WSe₂) exhibits long-range magnetic order, in which the V atoms induce both free holes and magnetic exchange at the valence band edge of WSe₂ [31,35,38]. Although remanence and magnetic domains have been observed in V-WSe₂ using a vibrating sample magnetometer and magnetic force microscopy, such characterization tools cannot provide the spin-polarized

*These authors contributed equally to this work.

†ddloc@skku.edu

‡leeyoung@skku.edu

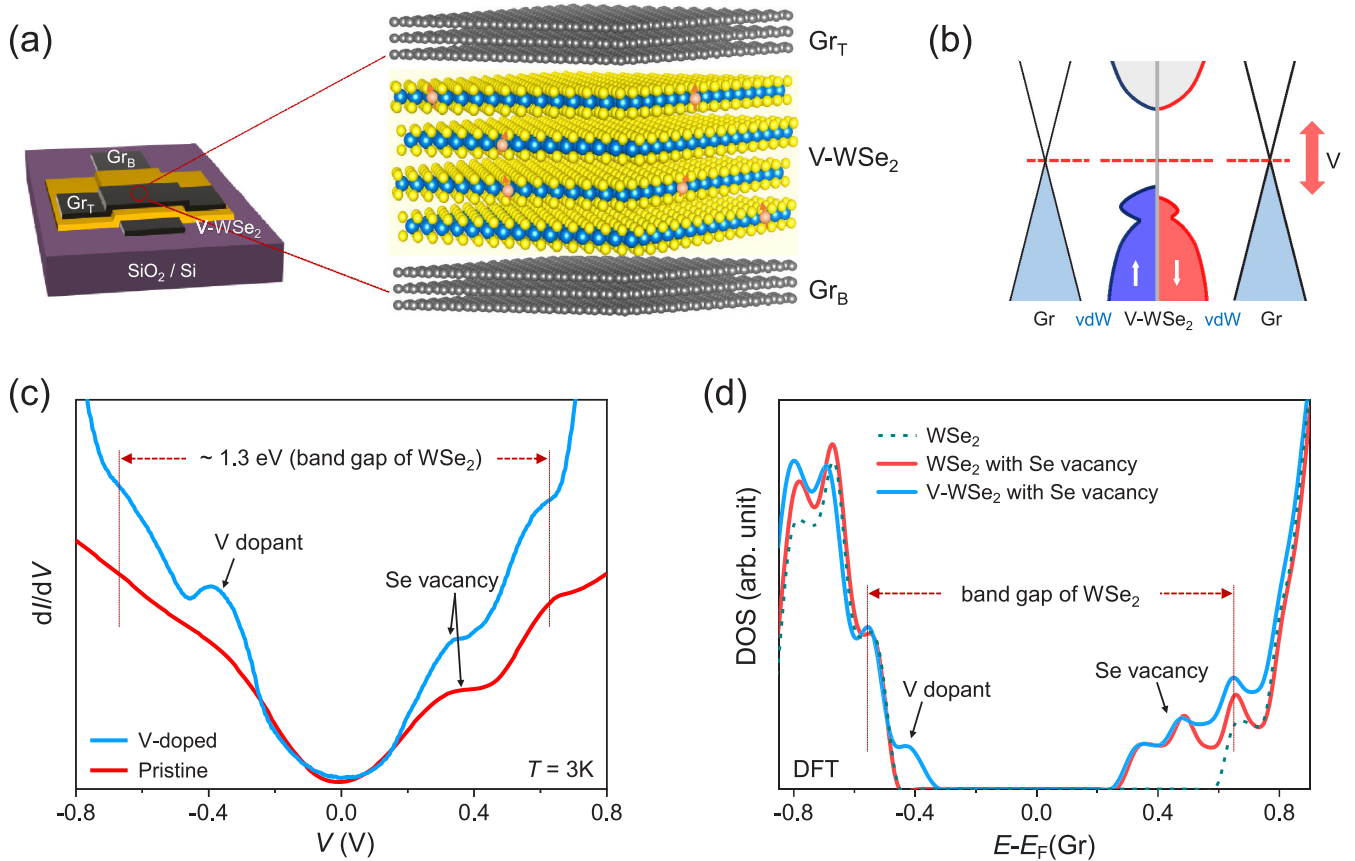


FIG. 1. Device structure and detection of the doping state. (a) Schematic illustration of the Gr_T/V-WSe₂/Gr_B tunneling junctions. (b) Band diagram of the device. (c) Comparison between the dI/dV curves of V-doped and pristine WSe₂ devices. (d) DFT calculation of the band structure of WSe₂ (dotted cyan), WSe₂ with Se vacancy (solid red), and V-doped WSe₂ with Se vacancy (solid blue), including spin-orbit coupling. Here, a 10×10 supercell of bilayer WSe₂ was used (with one V atom and one Se vacancy) for the calculation.

characteristics of free carriers [3]. Concrete evidence of long-range magnetic order with spin-polarized carriers should be obtained using reliable approaches such as magnetoelectrical transport.

In this work, we investigate the magnetoelectrical properties of multilayered V-doped WSe₂ by fabricating a vertical heterostructure of graphite/V-WSe₂/graphite. The sample was encapsulated by both top and bottom graphite layers to prevent oxidation. We observed a giant Zeeman shift of the V-dopant state located near the valence band edge by measuring the resonant magnetotunneling current, indicating the existence of strong magnetic exchange interactions of V, W, and Se atoms. These interactions appear at 300 K, and the ferromagnetic order is also detected up to 50 K at a low doping concentration of $x = 0.15\%$ (in the structure defined as V_xW_{1-x}Se₂) by conducting temperature-dependent resistance measurements and investigating the magnetoresistance (MR) hysteresis.

II. EXPERIMENTAL DETAILS

A. Preparation of materials

A single crystal of V-WSe₂ was synthesized via a two-step chemical vapor transport (CVT) method. The reactant powders with high purity, namely tungsten (W, 99.999%, Sigma Aldrich), selenium (Se, 99.998%, Sigma Aldrich), and vanadium (V, 99.99%, Sigma Aldrich), were mixed with each other and ground uniformly at a nominated ratio. The mixed powder was compressed to pellets prior to loading into the quartz ampule for sealing. After evacuation and sealing, the sealed ampule was placed in a box furnace for annealing at 950 °C for 24 h. Iodine was then added as a transporting agent for the second step of the CVT process, which was performed at 1000–1100 °C for 200 h. The pristine sample was processed similarly, except that the reactant powders were only tungsten and selenium.

dium (V, 99.99%, Sigma Aldrich), were mixed with each other and ground uniformly at a nominated ratio. The mixed powder was compressed to pellets prior to loading into the quartz ampule for sealing. After evacuation and sealing, the sealed ampule was placed in a box furnace for annealing at 950 °C for 24 h. Iodine was then added as a transporting agent for the second step of the CVT process, which was performed at 1000–1100 °C for 200 h. The pristine sample was processed similarly, except that the reactant powders were only tungsten and selenium.

B. Device fabrication and characterization

To investigate the magnetoelectrical properties of the crystal, we fabricated the device illustrated in Fig. 1(a). A 5–7-nm-thick V-WSe₂ flake, which was employed as a transport channel, was confined between two graphite flakes (~5 nm) that served as the top and bottom electrodes. The flakes were stacked using a dry transfer method. Specifically, we exfoliated thin graphite flakes on a Si/SiO₂ substrate as the bottom electrode (Gr_B), together with V-WSe₂ (in the lateral size of approximately 10–20 μm) and another graphite flake on a PVA/PMMA-coated substrate prepared for transfer. The V-WSe₂ flake was then stacked onto the bottom graphite electrode, after which the top graphite flake (Gr_T) was transferred and positioned on the V-WSe₂ channel. The atomic V dopant

concentration is approximately $x = 0.15\%$ (in the structure defined as $V_xW_{1-x}Se_2$) as measured by the electron probe microanalyzer (see Fig. S1 in Supplemental Material [42]).

This device structure has several advantages. The interface between the graphite and V-WSe₂ forms a van der Waals contact, which could avoid defect generation during the evaporation process in conventional metal deposition. Taking advantage of this van der Waals barrier between graphite and V-WSe₂, the resonant tunneling spectrum can be measured to verify the doping states at low temperatures [43,44]. Moreover, the top and bottom graphite electrodes can passivate the V-WSe₂ channel. Importantly, the vertical structure of the device prevents the resistance from increasing exponentially when lowering the temperature in planar semiconductor devices, which is normally beyond the detection range of measurement systems [45].

The electrical characteristics of the devices were examined using a physical property measurement system (PPMS, Quantum Design) in conjunction with an internal electrical transport option (ETO) module and external Keithley 4200 system. The dI/dV characteristics were measured by the ETO module of the PPMS at 3 K with an ac excitation of 0.01 V.

III. RESULTS

A. Probing the spin-polarized doping state

Figure 1(b) depicts the band diagram of the graphite/V-WSe₂/graphite device with the spin-polarized band of V-WSe₂. The hole dopant level of vanadium is supposed to exist near the valence band of WSe₂, as observed by scanning tunneling spectroscopy [46]. To confirm the doping states of V in WSe₂, we performed low-temperature dI/dV characterization of the pristine and V-doped WSe₂ vertical devices [Fig. 1(c)]. In the pristine WSe₂ device, two main peaks appear near the biases of approximately 0.3 V and 0.65 V, originating from the Se vacancy states and the bottom of the conduction band [47]. A clear peak indicating the top of the valence band in the negative bias range is not apparent because of the background current. However, by taking the derivative of the dI/dV curve, one peak-dip pair in the d^2I/dV^2 curve is observed near -0.65 V (see Fig. S2 in Supplemental Material [42]), indicating the top of the valence band. The difference between the bias positions corresponding to the edges of the conduction and valence bands matches well with the band gap value of approximately 1.3 eV for multilayered WSe₂ [48]. In the V-doped WSe₂ device, a noticeable additional peak appears at approximately -0.4 V (near the valence band) in the dI/dV curve, in addition to the three bias positions observed for the pristine sample. This feature is related to the doping state of the V atoms, which is in good agreement with the theoretical density functional theory (DFT) calculation, as shown in Fig. 1(d). (Details of the calculation can be found in our previous reports [32,49].) This feature has also been observed in a V-doped WSe₂ monolayer using a scanning tunneling microscope [46]. This new peak in the dI/dV curve confirms the hole-doping effect of vanadium in the WSe₂ host. Because both the pristine and V-doped WSe₂ devices exhibit a peak near 0.3 V, we attribute the origin of this peak to the Se vacancies.

To further verify the spin polarization of the doping state, we performed the dI/dV characterization under an external magnetic field (from 0–4 T in increments of 0.2 T), namely, the resonant magnetotunneling spectra (Fig. 2(a) and also see Fig. S3(a) in Supplemental Material [42] for the full set of curves) [44,50]. Interestingly, the defect state located at approximately -0.4 V is substantially shifted toward a higher negative bias under the applied magnetic field. To clearly reveal the peak shift, the first derivative of the dI/dV curves at 0, 1, 2, 3, and 4 T is further shown in Fig. 2(b) (see also Fig. S3(b) in Supplemental Material [42] for the full set of curves). We clearly observed one peak-dip pair in the d^2I/dV^2 curves corresponding to each peak in the dI/dV curves near -0.4 V. The shift of the peak near -0.4 V is approximately -7.8 meV/T for the dopant peak, as shown in Fig. 2(c). Such a large energy shift, even for an exceedingly small amount of V ($x = 0.15\%$ in $V_xW_{1-x}Se_2$), leads to a huge effective Landé factor (g_{eff}) of approximately 135, calculated from $\Delta E/\Delta B = g_{\text{eff}} \times \mu_B$, where the Bohr magneton $\mu_B = 5.79 \times 10^{-5}$ eV/T. This is the highest value reported to date for 2D materials and is comparable to that of highly doped 3D magnetic semiconductors such as Mn-doped CdSe; details regarding this appear in Table I [41,51–57]. In addition, the other peaks in the vicinity of -0.65 V and 0.65 V also shift by approximately -2.6 meV/T and 3.5 meV/T, respectively. These shifts are representative of the band edges of WSe₂, as shown in the d^2I/dV^2 mapping against the magnetic field [Fig. 2(d)]. The shift of the peak related to the Se vacancy at 0.3 V is also considerable, approximately 2.7 meV/T. The anomalous energy shifts with large effective g factors are attributed to the strong $pd - d$ exchange interaction between the V and W/Se atoms in the V-WSe₂ system, inducing the spin-polarized band edges of WSe₂ [41,51] (this will be discussed in more detail later). Our result shows the possibility of the realization of real DMSs with a minute content of dopant atoms in transition-metal dichalcogenides [58,59].

B. Probing long-range magnetic interaction and order

The characteristics of the magnetic interaction induced by the spin-polarized V dopant state were probed by investigating the resistance change with external magnetic fields. The measurement process, which is described in the schematic of Fig. 3(a), comprises four steps: (i) cooling in the absence of an external magnetic field (ZFC-C), (ii) heating in the absence of a magnetic field after ZFC-C (ZFC-H), (iii) cooling by applying a magnetic field (FC-C), and (iv) heating in the absence of a magnetic field after FC-C (FC-H). The main idea for this measurement process is to investigate the weakly interacting magnetic order under applying magnetic field. The occurrence of weak magnetic interactions can be determined by investigating the difference between the ZFC-H and FC-H measurements. A significant difference between the ZFC and FC measurements is typically manifested in spin disorder structures [60,61], spin-glass systems [62,63], and magnetic interlayer interactions [64]. In our V-doped WSe₂, the magnetic interactions among the spin clusters formed at the V atoms can be investigated by employing this process.

Figures 3(b) and 3(c) show the detailed ZFC and FC characteristics of V-doped WSe₂ and pristine WSe₂ as a control

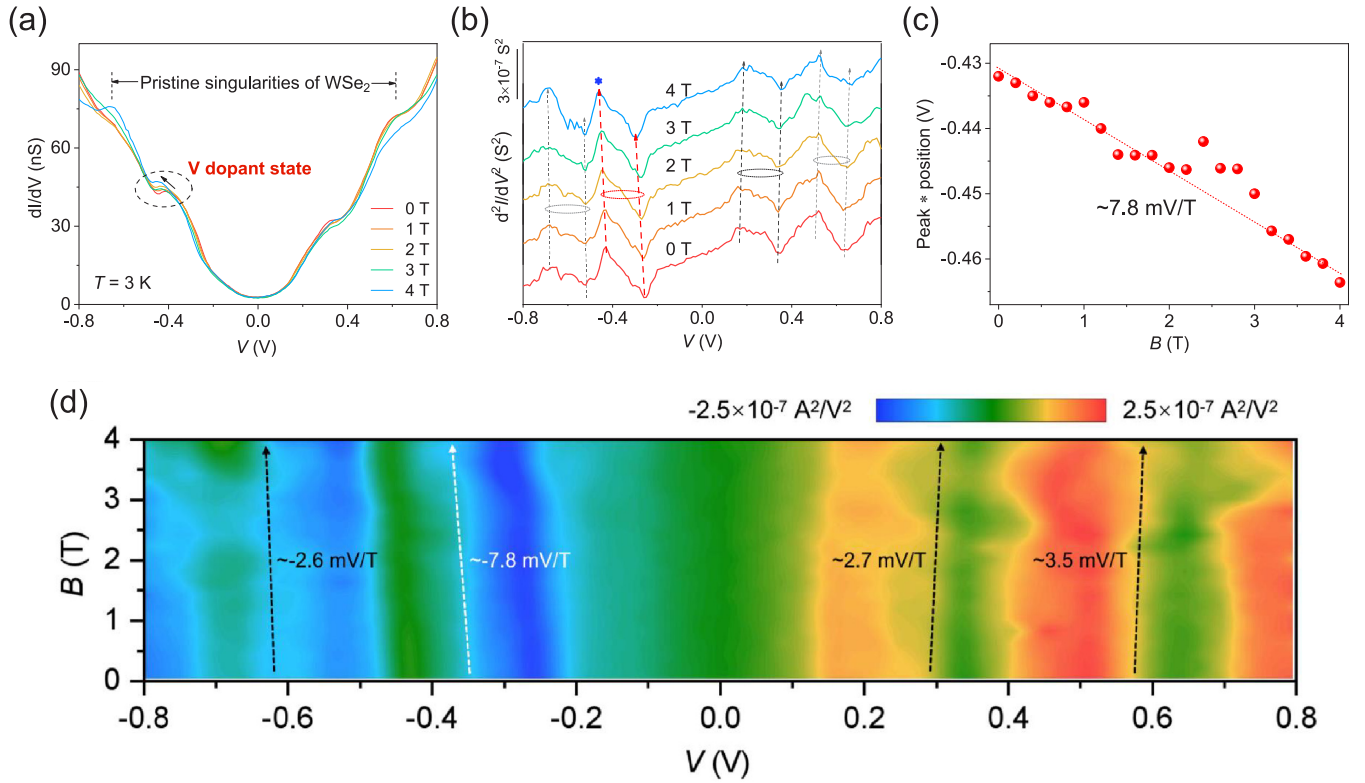


FIG. 2. Verification of the spin polarized nature of the doping state. (a) dI/dV curves and (b) d^2I/dV^2 curves of the V-WSe₂ device in the presence of a magnetic field of 0–4 T. (c) Shift in the peak position of the doping state as marked * in (b). (d) d^2I/dV^2 mapping against the magnetic field and bias.

study. The sample was first cooled from 400–3 K without applying a magnetic field (ZFC-C), and then heated to 400 K again (ZFC-H). We next applied the magnetic field (3 T) at 400 K, and then cooled the sample to 3 K in the presence of the magnetic field (FC-C). The magnetic field was then oscillated to 0 T. Finally, we heated the sample again to 400 K (FC-H). The resistance was measured during the entire process. In the V-doped WSe₂ sample, the resistance in the case of FC-C differs significantly from that in the case of ZFC-C, whereas the value is retained with the oscillatory magnetic field upon removal of the magnetic field at 3 K [Fig. 3(b-IV)], indicating the formation of an emerging magnetic order during the FC-C process. This remanence of magnetoresistance (the difference in resistance between the FC-H and ZFC-H) is persistent at ~ 300 K [Fig. 3(b-V)]. This implies that the magnetic interac-

tion between the spin clusters formed at the V atoms persists at room temperature. The average V-V distance at 0.15% is ~ 3.5 nm (equivalent to one V atom out of 100 unit cells). This strongly suggests that the magnetic exchange interaction between V atoms is long ranged and that it is established at 300 K. In contrast, conventional magnetoresistance exhibits no appreciable remanence in the pristine sample [Figs. 3(c-IV) and 3(c-V)].

Figure 4(a) depicts the difference in resistance between FC and ZFC during the heating process, $\delta = (R_{FC-H} - R_{ZFC-H})/R_{ZFC-H}$. Three temperature regimes are clearly distinguishable for the V-doped sample: (i) negligible δ above 300 K, marked as the freezing temperature T_F , (ii) gradual change of δ with temperature in the range $50 \text{ K} < T < 300 \text{ K}$, and (iii) saturated δ below 50 K, marked as the Curie

TABLE I. Comparison of the energy shift and g factor between the V-WSe₂ system and other related systems.

State	Method	Energy shift (meV T ⁻¹)	g_{eff}	Ref.	
V-WSe ₂	V-doping state	Resonant magnetotunneling spectrum	~ 7.8	~ 135	Our work
H atom/ electron		Spin-cyclotron difference frequency	0.11	~ 2	[52,53]
WSe ₂	Band edge	Polarization-resolved PL	0.1 ~ 0.2	1.725 ~ 3.75	[54,55]
Vanadium complexes	V energy levels	Electron paramagnetic resonance spectroscopy	~ 0.11	1.8 ~ 2.1	[56]
Fe-MoS ₂	Band edge	Polarization-resolved PL	1.2	20.7	[41]
Co-MoS ₂	Band edge	Polarization-resolved PL	0.87	15	[51]
CdSe	Band edge	Magnetic circular dichroism	0.1	1.725	[57]
Mn-CdSe	Band edge	Magnetic circular dichroism	~ 13 (average)	~ 220	[57]

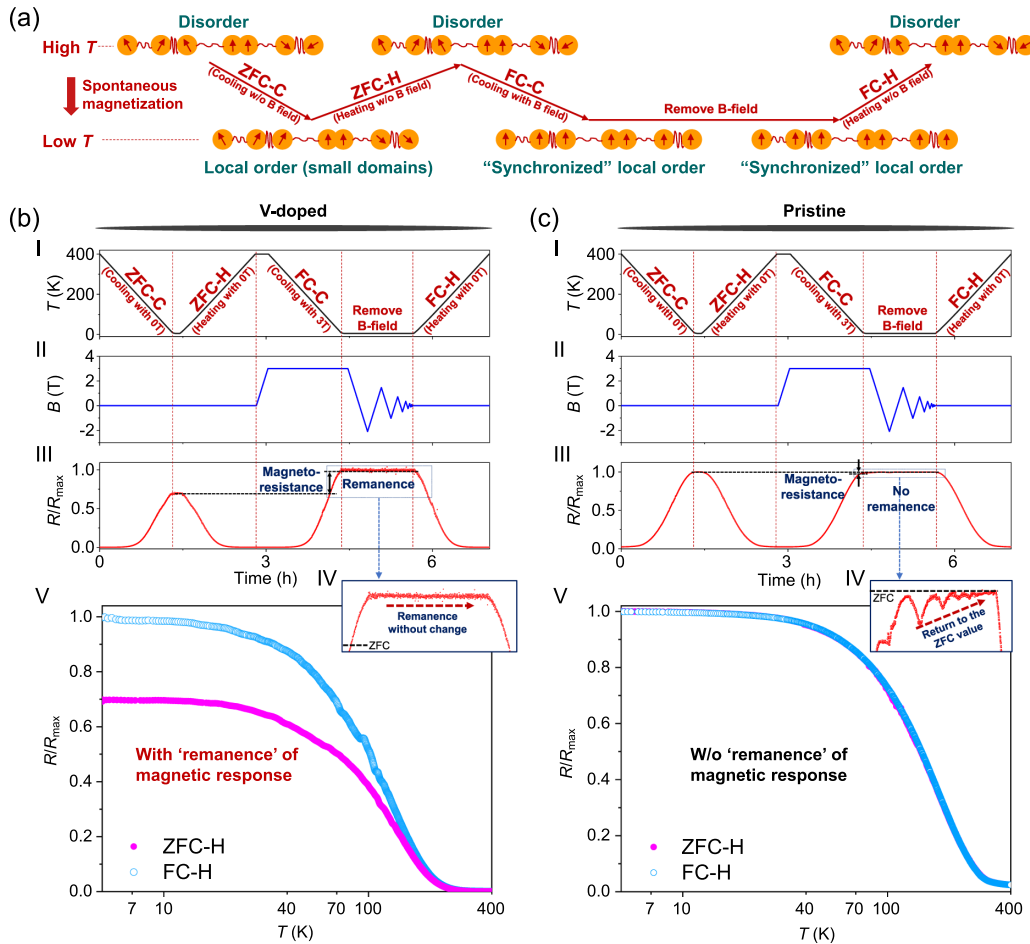


FIG. 3. Resistance characteristics of V-doped and pristine WSe₂ devices in ZFC and FC. (a) Schematic illustration of the ZFC and FC characterization processes and the changes in the spin structure. (b)–(c) Comparison between the V-doped WSe₂ (b) and pristine WSe₂ (c) devices with detailed resistance characterization during ZFC and FC processes. (b–I–III) and (c–I–III): the detailed ZFC and FC measurement processes of the corresponding V-doped and pristine WSe₂ devices. (b–IV) and (c–IV): zoomed-in view of the resistance changing with the oscillated magnetic field to 0 T at 3 K of the corresponding V-doped and pristine WSe₂ devices. For the V-doped sample, the resistance during the magnetic field oscillation to 0 T at 3 K is almost constant with the magnetic field change, maintaining a resistance remanence compared to that of ZFC. In contrast, the resistance of pristine WSe₂ follows the oscillated magnetic field and returns back to the resistance value of ZFC, indicating the pure magnetoresistance without remanence of pristine WSe₂. (b–V) and (c–V): difference between the ZFC-H and FC-H curves of the corresponding V-doped and pristine WSe₂ devices with the normalized resistance (R/R_{\max}) as the y axis.

temperature T_C . In contrast, the difference in resistance between FC and ZFC was not clearly observed for the pristine sample. Because the V dopant atoms are randomly distributed inside the WSe₂ host, the magnetic order transition occurs across a wide range of temperatures. This transition is similar to the glass transition [65]. The spin-glass transition starts at T_F and ends at T_C . The magnetic interaction between spin clusters is established below T_C . This is similar to the behavior of magnetic susceptibility in magnetic spin-glass systems [66]. We note that the T_F may change with V concentration (see Fig. S4 in Supplemental Material [42]).

Next, we extract the first derivative of the R – T curves with the ZFC–C process. Two peaks (P1, P2) in the dR/dT curve are clearly visible in the doped sample, in contrast with the single peak (P1) in the pristine WSe₂ [Fig. 4(a)]. P1, which is observed for both the doped and pristine WSe₂ devices, originates from the transition between thermionic-emission-dominated transport and tunneling-dominated trans-

port regimes as discussed in Fig. S5 in Supplemental Material [42] (see, also, references [67,68] therein). The new peak P2 coincides with T_C of the dR/dT – T curve, as shown in Fig. 4(a). As mentioned above, during the ZFC–C process, local magnetic spins can be oriented owing to the spontaneous alignment process associated with the magnetic scattering centers in V–WSe₂ below T_C , which is manifested by the P2 peak on the dR/dT curve [3,64]. To probe the magnetic order in the V–WSe₂ sample, the hysteresis in the magnetoresistance curves was further investigated at different temperatures. In the temperature range of 2–50 K, hysteresis is clearly observed in the magnetoresistance curves [Figs. 4(b) and 4(c)]. Meanwhile, the hysteresis of the magnetoresistance cannot be probed owing to the drift of the resistance with time at higher temperatures [Fig. 4(d)]. Such a resistance drift is attributed to the degradation of the ferromagnetic order with time, implying nature of the spin-glass transition at above 50 K. Ferromagnetism exists below the T_C (approximately 50

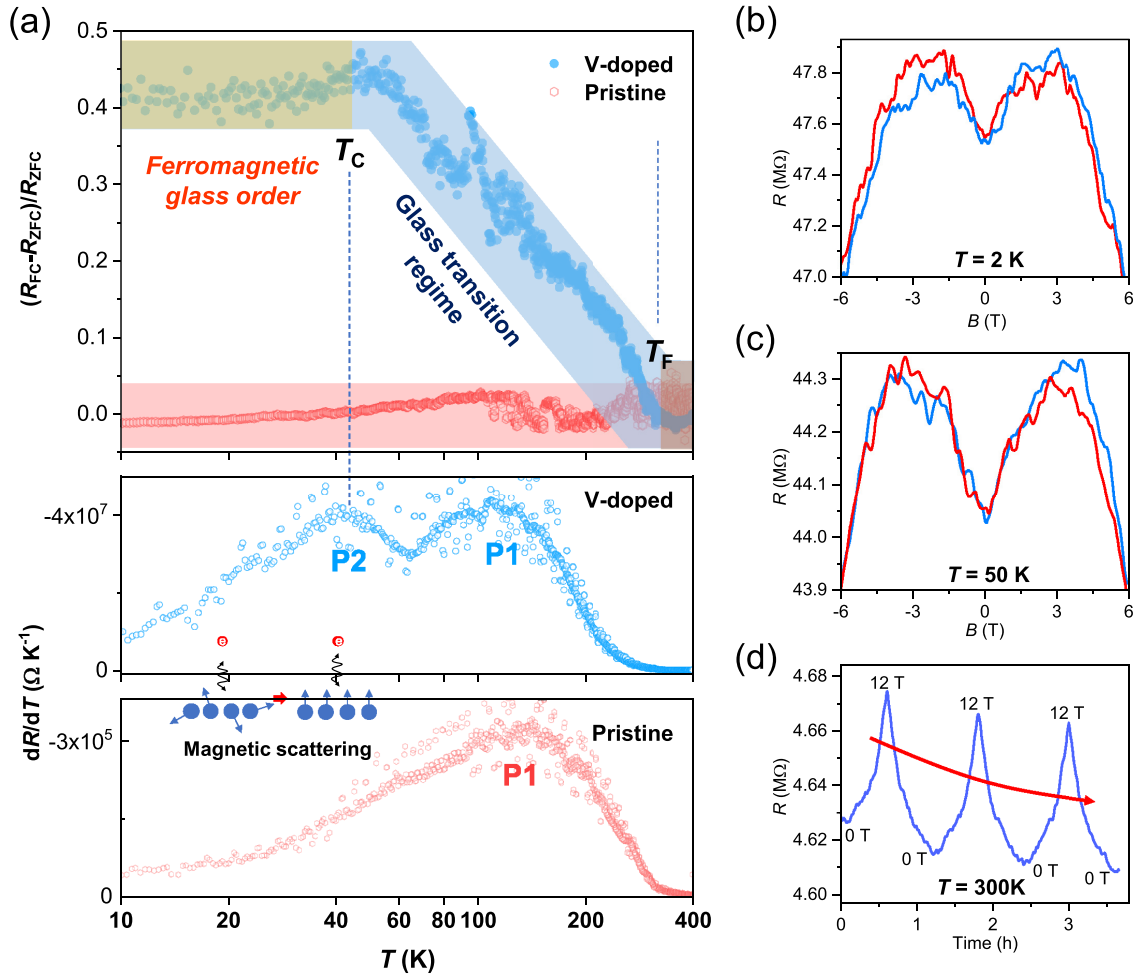


FIG. 4. Magnetic transition of V-doped WSe_2 . (a) Comparison between $(R_{FC-H} - R_{ZFC-H})/R_{ZFC-H} - T$ and $dR/dT - T$ curves of the V-doped and pristine WSe_2 devices to verify the magnetic transition. Inset: schematic of the change in the magnetic scattering due to the spin alignment. (b)–(c) Magnetoresistance of V- WSe_2 device at 2 K (b) and 50 K (c). (d) Time evolution of the resistance measured with the magnetic field scanning of V- WSe_2 device at 300 K.

K) in the V- WSe_2 sample. We would like to note that T_C for the multilayered sample is lower than that of the reported monolayer case [35], which could be attributed to the doping effect of the graphite electrodes to the V-doped WSe_2 , reducing the hole concentration in the sample. The thickness and contribution of Se vacancies can be other possible reasons for the difference.

C. Spin-polarized and non-spin-polarized states in V- WSe_2

The existence of spin-polarized states and long-range magnetic interactions reveals the nature of the magnetism in V- WSe_2 . Nevertheless, V atoms cannot be fully spin-polarized in the entire band structure of WSe_2 . Typically, the spin-polarized energy levels appear within ~ 0.5 eV from the conduction or valence band edge between the V and W or Se atoms [32,49]. Figure 5(a) shows the spin-up and spin-down density of states of the V- WSe_2 bilayer. The difference between these two types of density of states or polarized spins clearly indicates the existence of spin-polarized states near the valence band edge. Notably, the highly polarized spin becomes prominent within 0.5 eV below the valence band edge,

similar to the case of the V- WSe_2 monolayer [32,49]. This polarized spin becomes less obvious at energy levels far from the valence band edge. To experimentally verify this effect, we investigated δ by varying the bias. The Fermi levels in both graphite electrodes in the Gr/V- WSe_2 /Gr device undergo a shift when the bias changes. The spin-up density of states differs from the spin-down states near the valence band edge of V- WSe_2 . Far away from the valence band edge, the spin-polarized bands are weaker. By varying the bias, it becomes possible to control the extent to which the spin-polarized states are involved in the electrical transport, which enables the modulation of the magnetoresistance between the FC and ZFC curves, as shown in Figs. 5(b)–5(d). With a small bias at $V = -0.1$ V, the difference in resistance between the ZFC and FC curves, which is determined by the contribution of the spin-polarized states of V- WSe_2 , is very small [Fig. 5(b), bottom panel]. It implies the main contribution to the resistance is from the direct tunneling between the top and bottom graphite electrodes with a nonnegligible involvement of the density of states of V- WSe_2 (see Fig. S6 in Supplemental Material [42] for the detailed analysis). In contrast, applying a medium bias (e.g., -0.4 V) gives rise to a substantial difference in

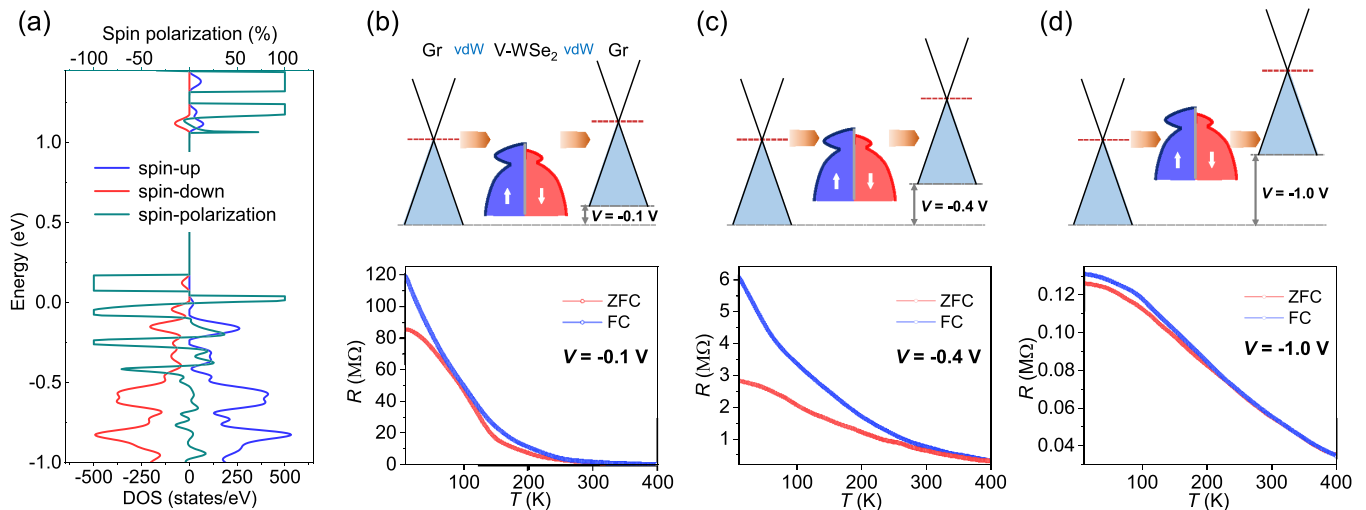


FIG. 5. Distinguishing spin-polarized states with applied voltage. (a) Spin-polarized density of states of V-doped WSe₂. Highly spin-polarized states are revealed within 0.5 eV below the valence band edge. (b)–(d) Band diagrams of Gr/V-WSe₂/Gr device at -0.1 V (b), -0.4 V (c), and -1.0 V (d) with corresponding modulation of the R - T curves of ZFC and FC processes. Location of spin-polarized states in the bias windows can be modulated by varying the applied bias. More density of states of V-WSe₂ are involved in transport by increasing the bias (c), but the contribution of non-spin-polarized states become dominant in the case of a large bias (d).

resistance between the ZFC and FC curves [Fig. 5(c)]. At this bias, the main contribution of the current is the tunneling current through the top graphite electrode, V-WSe₂, and the bottom graphite electrode via the spin-polarized states of V-WSe₂. Increasing the applied bias (e.g., to -1 V) involves a heavier density of states of V-WSe₂, but the contribution of non-spin-polarized states inside the valence band is reduced [Fig. 5(d)], also resulting in a small difference in the resistance between the ZFC and FC curves.

IV. CONCLUSIONS

In summary, we electrically probed the magnetism of multilayered V-doped WSe₂ flakes with vertically stacked graphite/V-WSe₂/graphite heterojunction devices. The V

dopant, which introduces p -type doping into the WSe₂ host, features the spin-polarized state via resonant magnetotunneling transport. A large Zeeman energy shift of the doping state and the band edges induced by a strong pd - d exchange interaction is observed, indicating the DMS nature of V-WSe₂. Long-range magnetic exchange is maintained up to 300 K with a substantial V-V distance of approximately 3.5 nm. An in-depth understanding of the nature of the V-WSe₂ system provides opportunities for future spintronics based on 2D van der Waals DMSs.

ACKNOWLEDGMENT

This work was supported by the Institute for Basic Science of Korea (IBS-R011-D1).

- [1] H. Ohno, D. Chiba, F. Matsukura, T. Omiya, E. Abe, T. Dietl, Y. Ohno, and K. Ohtani, Electric-field control of ferromagnetism, *Nature (London)* **408**, 944 (2000).
- [2] D. D. Awschalom and R. K. Kawakami, Teaching magnets new tricks, *Nature (London)* **408**, 923 (2000).
- [3] A. MacDonald, P. Schiffer, and N. Samarth, Ferromagnetic semiconductors: moving beyond (Ga,Mn)As, *Nature Mater.* **4**, 195 (2005).
- [4] A. Bonanni and T. Dietl, A story of high-temperature ferromagnetism in semiconductors, *Chem. Soc. Rev.* **39**, 528 (2010).
- [5] D. Chiba, M. Sawicki, Y. Nishitani, Y. Nakatani, F. Matsukura, and H. Ohno, Magnetization vector manipulation by electric fields, *Nature (London)* **455**, 515 (2008).
- [6] A. Chernyshov, M. Overby, X. Liu, J. K. Furdyna, Y. Lyanda-Geller, and L. P. Rokhinson, Evidence for reversible control of magnetization in a ferromagnetic material by means of spin-orbit magnetic field, *Nat. Phys.* **5**, 656 (2009).
- [7] F. Matsukura, Y. Tokura, and H. Ohno, Control of magnetism by electric fields, *Nat. Nanotechnol.* **10**, 209 (2015).
- [8] S. Ikeda, K. Miura, H. Yamamoto, K. Mizunuma, H. D. Gan, M. Endo, S. Kanai, J. Hayakawa, F. Matsukura, and H. Ohno, A perpendicular-anisotropy CoFeB-MgO magnetic tunnel junction, *Nat. Mater.* **9**, 721 (2010).
- [9] Ø. Johansen, V. Risinggård, A. Sudbø, J. Linder, and A. Brataas, Current Control of Magnetism in Two-Dimensional Fe₃GeTe₂, *Phys. Rev. Lett.* **122**, 217203 (2019).
- [10] C. Zener, Interaction between the D shells in the transition metals, *Phys. Rev.* **81**, 440 (1951).
- [11] M. J. Calderón, G. Gómez-Santos, and L. Brey, Impurity-semiconductor band hybridization effects on the critical temperature of diluted magnetic semiconductors, *Phys. Rev. B* **66**, 075218 (2002).
- [12] S. D. Sarma, E. Hwang, and A. Kaminski, How to make semiconductors ferromagnetic: a first course on spintronics, *Solid State Commun.* **127**, 99 (2003).
- [13] T. Dietl and H. Ohno, Dilute ferromagnetic semiconductors: physics and spintronic structures, *Rev. Mod. Phys.* **86**, 187 (2014).

- [14] M. A. Ruderman and C. Kittel, Indirect exchange coupling of nuclear magnetic moments by conduction electrons, *Phys. Rev.* **96**, 99 (1954).
- [15] T. Dietl, A. Haury, and Y. M. d'Aubigné, Free carrier-induced ferromagnetism in structures of diluted magnetic semiconductors, *Phys. Rev. B* **55**, R3347 (1997).
- [16] T. Dietl, H. Ohno, F. Matsukura, J. Cibert, and E. D. Ferrand, Zener model description of ferromagnetism in zinc-blende magnetic semiconductors, *Science* **287**, 1019 (2000).
- [17] J. König, H.-H. Lin, and A. H. MacDonald, Theory of Diluted Magnetic Semiconductor Ferromagnetism, *Phys. Rev. Lett.* **84**, 5628 (2000).
- [18] T. Kasuya, A theory of metallic ferro- and antiferromagnetism on zener's model, *Prog. Theor. Phys.* **16**, 45 (1956).
- [19] H. Ohno, A. Shen, F. Matsukura, A. Oiwa, A. Endo, S. Katsumoto, and Y. Iye, (Ga,Mn)As: a new diluted magnetic semiconductor based on GaAs, *Appl. Phys. Lett.* **69**, 363 (1996).
- [20] H. Ohno, Making nonmagnetic semiconductors ferromagnetic, *Science* **281**, 951 (1998).
- [21] K. Wang, R. Campion, K. Edmonds, M. Sawicki, T. Dietl, C. Foxon, and B. Gallagher, Magnetism in (Ga,Mn)As Thin Films with T_C up to 173 K, *AIP Conf. Proc.* **772**, 333 (2005).
- [22] T. Jungwirth, K. Wang, J. Mašek, K. W. Edmonds, J. König, J. Sinova, M. Polini, N. A. Goncharuk, A. H. MacDonald, M. Sawicki, A. W. Rushforth, R. P. Campion, L. X. Zhao, C. T. Foxon, and B. L. Gallagher, Prospects for high temperature ferromagnetism in (Ga,Mn)As semiconductors, *Phys. Rev. B* **72**, 165204 (2005).
- [23] M. Wang, R. Campion, A. Rushforth, K. Edmonds, C. Foxon, and B. Gallagher, Achieving high curie temperature in (Ga,Mn)As, *Appl. Phys. Lett.* **93**, 132103 (2008).
- [24] T. Dietl, A ten-year perspective on dilute magnetic semiconductors and oxides, *Nature Mater.* **9**, 965 (2010).
- [25] A. Van Esch, L. Van Bockstal, J. De Boeck, G. Verbanck, A. S. van Steenberghe, P. J. Wellmann, B. Grietens, R. Bogaerts, F. Herlach, and G. Borghs, Interplay between the magnetic and transport properties in the III-V diluted magnetic semiconductor $Ga_{1-x}Mn_xAs$, *Phys. Rev. B* **56**, 13103 (1997).
- [26] S. Ohya, K. Takata, and M. Tanaka, Nearly non-magnetic valence band of the ferromagnetic semiconductor GaMnAs, *Nat. Phys.* **7**, 342 (2011).
- [27] N. Samarth, Battle of the bands, *Nat. Mater.* **11**, 360 (2012).
- [28] R. Mishra, W. Zhou, S. J. Pennycook, S. T. Pantelides, and J.-C. Idrobo, Long-range ferromagnetic ordering in manganese-doped two-dimensional dichalcogenides, *Phys. Rev. B* **88**, 144409 (2013).
- [29] K. Zhang, S. Feng, J. Wang, A. Azcatl, N. Lu, R. Addou, N. Wang, C. Zhou, J. Lerach, V. Bojan, M. J. Kim, L.-Q. Chen, R. M. Wallace, M. Terrones, J. Zhu, and J. A. Robinson, Manganese doping of monolayer MoS_2 : the substrate is critical, *Nano Lett.* **15**, 6586 (2015).
- [30] B. Li, T. Xing, M. Zhong, L. Huang, N. Lei, J. Zhang, J. Li, and Z. Wei, A two-dimensional Fe-doped SnS_2 magnetic semiconductor, *Nature Commun.* **8**, 1 (2017).
- [31] S. J. Yun, D. L. Duong, M.-H. Doan, K. Singh, T. L. Phan, W. Choi, Y.-M. Kim, and Y. H. Lee, Room-Temperature Ferromagnetism in Monolayer WSe_2 Semiconductor via Vanadium Dopant, [arXiv:1806.06479](https://arxiv.org/abs/1806.06479).
- [32] D. L. Duong, S. J. Yun, Y. Kim, S.-G. Kim, and Y. H. Lee, Long-range ferromagnetic ordering in vanadium-doped WSe_2 semiconductor, *Appl. Phys. Lett.* **115**, 242406 (2019).
- [33] Y. Gao, N. Ganguli, and P. J. Kelly, Itinerant ferromagnetism in p-doped monolayers of MoS_2 , *Phys. Rev. B* **99**, 220406(R) (2019).
- [34] L. Yang, H. Wu, W. Zhang, X. Lou, Z. Xie, X. Yu, Y. Liu, and H. Chang, Ta doping enhanced room-temperature ferromagnetism in 2D semiconducting $MoTe_2$ nanosheets, *Adv. Electron. Mater.* **5**, 1900552 (2019).
- [35] S. J. Yun, D. L. Duong, D. M. Ha, K. Singh, T. L. Phan, W. Choi, Y.-M. Kim, and Y. H. Lee, Ferromagnetic order at room temperature in monolayer WSe_2 semiconductor via vanadium dopant, *Adv. Sci.* **7**, 1903076 (2020).
- [36] S. Fu, K. Kang, K. Shayan, A. Yoshimura, S. Dadras, X. Wang, L. Zhang, S. Chen, N. Liu, A. Jindal, X. Li, A. N. Pasupathy, A. N. Vamivakas, V. Meunier, S. Strauf, and E.-H. Yang, Enabling room temperature ferromagnetism in monolayer MoS_2 via in situ iron-doping, *Nat. Commun.* **11**, 1 (2020).
- [37] S. Ahmed, X. Ding, P. P. Murmu, N. Bao, R. Liu, J. Kennedy, L. Wang, J. Ding, T. Wu, A. Vinu, and J. Yi, High coercivity and magnetization in WSe_2 by codoping Co and Nb, *Small* **16**, 1903173 (2020).
- [38] Y. T. H. Pham, M. Liu, V. O. Jimenez, F. Zhang, V. Kalappattil, Z. Yu, K. Wang, T. Williams, M. Terrones, and M.-H. Phan, Tunable ferromagnetism and thermally induced spin flip in vanadium-doped tungsten diselenide monolayers at room temperature, *Adv. Mater.* **32**, 2003607 (2020).
- [39] Y. Cheng, Z. Zhu, W. Mi, Z. Guo, and U. Schwingenschlögl, Prediction of two-dimensional diluted magnetic semiconductors: doped monolayer MoS_2 systems, *Phys. Rev. B* **87**, 100401(R) (2013).
- [40] A. Ramasubramaniam and D. Naveh, Mn-doped monolayer MoS_2 : an atomically thin dilute magnetic semiconductor, *Phys. Rev. B* **87**, 195201 (2013).
- [41] Q. Li, X. Zhao, L. Deng, Z. Shi, S. Liu, Q. Wei, L. Zhang, Y. Cheng, L. Zhang, H. Lu, W. Gao, W. Huang, C.-W. Qiu, G. Xiang, S. J. Pennycook, Q. Xiong, K. P. Loh, and B. Peng, Enhanced valley zeeman splitting in Fe-doped monolayer MoS_2 , *ACS Nano* **14**, 4636 (2020).
- [42] See Supplemental Material at <http://link.aps.org/supplemental/10.1103/PhysRevB.103.014441> for detailed evaluation of the V concentration of CVT samples; d^2I/dV^2 curve of the pristine WSe_2 device; full set of the dI/dV and d^2I/dV^2 curves of the V- WSe_2 device under the magnetic field; plot of the freezing temperatures (T_F) vs V concentrations; and discussion on the transport mechanism of our heterostructure devices.
- [43] D. Ghazaryan, M. T. Greenaway, Z. Wang, V. H. Guarochico-Moreira, I. J. Vera-Marun, J. Yin, Y. Liao, S. V. Morozov, O. Kristanovski, A. I. Lichtenstein, M. I. Katsnelson, F. Withers, A. Mishchenko, L. Eaves, A. K. Geim, K. S. Novoselov, and A. Misra, Magnon-assisted tunnelling in van der Waals heterostructures based on $CrBr_3$, *Nat. Electron.* **1**, 344 (2018).
- [44] N. Akiba, F. Matsukura, Y. Ohno, A. Shen, K. Ohtani, T. Sakon, M. Motokawa, and H. Ohno, Magnetotunneling spectroscopy of resonant tunneling diode using ferromagnetic (Ga,Mn)As, *Physica B* **256**, 561 (1998).
- [45] D. H. Luong, T. L. Phan, G. Ghimire, D. L. Duong, and Y. H. Lee, Revealing antiferromagnetic transition of van der Waals

- MnPS₃ via vertical tunneling electrical resistance measurement, *APL Mater.* **7**, 081102 (2019).
- [46] B. Song, S. J. Yun, J. Jiang, K. Beach, W. Choi, Y.-M. Kim, H. Terrones, Y. J. Song, D. L. Duong, and Y. H. Lee, Evidence of Itinerant Holes for Long-Range Magnetic Order in Tungsten Diselenide Semiconductor with Vanadium Dopants, [arXiv:2002.07333](https://arxiv.org/abs/2002.07333).
- [47] M. Tosun, L. Chan, M. Amani, T. Roy, G. H. Ahn, P. Taheri, C. Carraro, J. W. Ager, R. Maboudian, and A. Javey, Air-stable n-doping of WSe₂ by anion vacancy formation with mild plasma treatment, *ACS Nano* **10**, 6853 (2016).
- [48] J. A. Wilson and A. Yoffe, The transition metal dichalcogenides discussion and interpretation of the observed optical, electrical and structural properties, *Adv. Phys.* **18**, 193 (1969).
- [49] D. L. Duong, S.-G. Kim, and Y. H. Lee, Gate modulation of the long-range magnetic order in a vanadium-doped WSe₂ semiconductor, *AIP Adv.* **10**, 065220 (2020).
- [50] Le Duc Anh, P. N. Hai, and M. Tanaka, Observation of spontaneous spin-splitting in the band structure of an n-type zinc-blende ferromagnetic semiconductor, *Nat. Commun.* **7**, 13810 (2016).
- [51] J. Zhou, J. Lin, H. Sims, C. Jiang, C. Cong, J. A. Brehm, Z. Zhang, L. Niu, Y. Chen, Y. Zhou, Y. Wang, F. Liu, C. Zhu, T. Yu, K. Suenaga, R. Mishra, S. T. Pantelides, Z.-G. Zhu, W. Gao, Z. Liu, and W. Zhou, Synthesis of co-doped MoS₂ monolayers with enhanced valley splitting, *Adv. Mater.* **32**, 1906536 (2020).
- [52] R. S. Van Dyck, P. B. Schwinberg, and H. G. Dehmelt, New High-Precision Comparison of Electron And Positron g Factors, *Phys. Rev. Lett.* **59**, 26 (1987).
- [53] B. Odom, D. Hanneke, B. D'Urso, and G. Gabrielse, New Measurement of the Electron Magnetic Moment Using a One-Electron Quantum Cyclotron, *Phys. Rev. Lett.* **97**, 030801 (2006).
- [54] A. Srivastava, M. Sidler, A. V. Allain, D. S. Lembke, A. Kis, and A. Imamoglu, Valley zeeman effect in elementary optical excitations of monolayer WSe₂, *Nat. Phys.* **11**, 141 (2015).
- [55] G. Aivazian, Z. Gong, A. M. Jones, R.-L. Chu, J. Yan, D. G. Mandrus, C. Zhang, D. Cobden, W. Yao, and X. Xu, Magnetic control of valley pseudospin in monolayer WSe₂, *Nat. Phys.* **11**, 148 (2015).
- [56] J. Krzystek, A. Ozarowski, J. Telser, and D. C. Crans, High-frequency and-field electron paramagnetic resonance of vanadium (IV, III, and II) complexes, *Coord. Chem. Rev.* **301**, 123 (2015).
- [57] J. H. Yu, X. Liu, K. E. Kweon, J. Joo, J. Park, K.-T. Ko, D. W. Lee, S. Shen, K. Tivakornsasithorn, J. S. Son, J.-H. Park, Y.-W. Kim, G. S. Hwang, M. Dobrowolska, J. K. Furdyna, and T. Hyeon, Giant zeeman splitting in nucleation-controlled doped CdSe:Mn²⁺ quantum nanoribbons, *Nat. Mater.* **9**, 47 (2010).
- [58] J. K. Furdyna, Diluted magnetic semiconductors, *J. Appl. Phys.* **64**, R29 (1988).
- [59] P. I. Archer, S. A. Santangelo, and D. R. Gamelin, Direct observation of sp-d exchange interactions in colloidal Mn²⁺- and Co²⁺-doped CdSe quantum dots, *Nano Lett.* **7**, 1037 (2007).
- [60] J. Greedan, M. Sato, X. Yan, and F. Razavi, Spin-glass-like behavior in Y₂Mo₂O₇, a concentrated, crystalline system with negligible apparent disorder, *Solid State Commun.* **59**, 895 (1986).
- [61] C. Tien, C. H. Feng, C. S. Wur, and J. J. Lu, Ce₂CuGe₃: A nonmagnetic atom-disorder spin glass, *Phys. Rev. B* **61**, 12151 (2000).
- [62] A. Maignan, A. Sundaresan, U. Varadaraju, and B. Raveau, Magnetization relaxation and aging in spin-glass (La, Y)_{1-x}Ca_xMnO₃ (x = 0.25, 0.3, and 0.5) perovskite, *J. Magn. Magn. Mater.* **184**, 83 (1998).
- [63] K. Binder and A. P. Young, Spin glasses: experimental facts, theoretical concepts, and open questions, *Rev. Mod. Phys.* **58**, 801 (1986).
- [64] D. R. Klein, D. MacNeill, J. L. Lado, D. Soriano, E. Navarro-Moratalla, K. Watanabe, T. Taniguchi, S. Manni, P. Canfield, J. Fernández-Rossier, and P. Jarillo-Herrero, Probing magnetism in 2D van der Waals crystalline insulators via electron tunneling, *Science* **360**, 1218 (2018).
- [65] J. C. Dyre, Colloquium: the glass transition and elastic models of glass-forming liquids, *Rev. Mod. Phys.* **78**, 953 (2006).
- [66] P. Joy, P. A. Kumar, and S. Date, The relationship between field-cooled and zero-field-cooled susceptibilities of some ordered magnetic systems, *J. Phys.: Condens. Matter* **10**, 11049 (1998).
- [67] S. Das, H.-Y. Chen, A. V. Penumatcha, and J. Appenzeller, High performance multilayer MoS₂ transistors with scandium contacts, *Nano Lett.* **13**, 100 (2013).
- [68] T. Ikuno, H. Okamoto, Y. Sugiyama, H. Nakano, F. Yamada, and I. Kamiya, Electron transport properties of Si nanosheets: transition from direct tunneling to fowler-nordheim tunneling, *Appl. Phys. Lett.* **99**, 023107 (2011).